# Low-frequency dielectric response in two-dimensional layered $MoO_3$ system doped with $Nb_2O_5$ at low temperatures

**S. Al-Khawaja[1,*] and M. Kassem[2]**

[1]Department of Physics and [2]Department of Chemistry,
Atomic Energy Commission of Syria, Damascus, P.O. Box 6091, Syria

**The AC electric conductivity has been studied for different bulk samples of molybdenum oxide ($MoO_3$) doped with niobium pentaoxide ($Nb_2O_5$). The dielectric constant curves have been obtained as a function of frequency (10 kHz < $f$ < 6 MHz) and temperature (80 ≤ $T$ ≤ 300 K). According to the dopant concentration, these compounds have been witnessed to exhibit a mild relaxation process in their dielectric constant. The behaviour is thought to be electronically attributed to excess oxygen vacancies and the thermally activated ionic conduction mechanism, occurring in the solid material formed upon doping with $Nb_2O_5$, which is utterly diffused into the layered structure of $MoO_3$ as the molar ratio $Nb_2O_5/MoO_3$ optimally reaches 0.4, associated with the abolishment of the two-dimensional structure.**

**Keywords:** Ceramic oxides, dielectric relaxation, ionic conductivity, layered structure.

THE molybdenum oxide ($MoO_3$) materials are amongst the transition metal oxide compounds that play a significant role in industrial applications, due to their physiochemical properties, nature of their structure and characteristics of their outer-shell electrons. Such oxides are used as catalysts in numerous chemical reactions in which, particularly, hydrogen or oxygen is participating[1]. They are also employed as optical electrochromic materials[2], and can be widely utilized in the partial oxidation of hydrocarbonates and alcohols, as well as in hydrogen treatment reactions conducted in the oil industry[3–6]. The catalytic properties of the active phase of $MoO_3$ are greatly influenced by the nature of the support oxide and dispersion of the active compound. The majority of these oxides are usually born on alumina, silica, titania, zerconia and vanadium oxide[7,8]. Moreover, these layered compounds have a significant role from the applied physical perspective in addition to their chemical utilization in the catalytic and oxidation reactions. They exhibit ferroelectric properties and may be considered as a charge density wave (CDW) system as well, with $MoO_6$ unit cells playing the fundamental constituent in their structure. Quantum Hartree–Fock and density functional theory calculations of the Hamiltonians performed on such compounds illustrate that the most crucial factor in the bonding is the electrostatic attraction between metal and oxygen atoms, in addition to a severe localized covalent contribution between the metal and single oxygen ligand[9]. The occurrence of this covalence is a prime impetus to cause symmetry reduction from the cubic to the tetragonal phase, which electronically participates in the transition from insulating to semiconducting or insulating to metallic state. Several publications on $MoO_3$ doped with alkali elements, particularly potassium molybdenum bronze, $K_{0.3}MoO_3$, also refer to the existence of a CDW-driven phase transition at 180 K, beneath which nonlinear current–voltage characteristics are realized[10]. The CDW conduction properties on the other hand, are greatly influenced by impurities existing haphazardly or intentionally in the structure of the material, like when doped with tungsten whereby the coherence length of CDW becomes extremely short for low concentrations of tungsten. Furthermore, the dielectric response function $\varepsilon(\omega) = \varepsilon' + i\varepsilon''$ has attracted attention and been the focus of several studies in low and high frequencies at low temperatures between 10 and 70 K in the pinned state of CDW of such oxides[11]. It has been demonstrated that the frequency response spectrum of the polarizability in the microwave region (higher than 1 GHz) can well be modelled with an overdamped Lorentzian oscillator. On the other hand, the response of the semiconducting material $K_{0.3}MoO_3$ in the low frequency region (less than 10 MHz) has been found to be strongly dispersive and dependent on temperature[11]. The dielectric behaviour measurements on the 'blue bronze' $K_{0.3}MoO_3$ by Jie and Ong[11] between 10 and 40 K for low frequencies $1 < \omega < 10$ kHz also indicate a broad and well-defined dielectric function, $\varepsilon(\omega)$, becoming more pronounced with decreasing temperature. At a temperature below 25 K, the results refer to the dielectric function increasing to very large values as both $\omega$ and $T$ tend towards zero. The latter findings have been interpreted on the basis of the Littlewood model, which identifies the low frequency mode according to a longitudinal response related to pinned CDWs[12]. It is worth mentioning that scanning tunnelling microscopy (STM) experiments have also been conducted to pinpoint the CDW phase in the quasi one-dimensional $Rb_{0.3}MoO_3$ compound[13].

Several papers focusing on the dielectric properties have also demonstrated the physical diversity of ceramic materials[11–15], with different interpretations proposed to explain their behaviour. In this communication, $MoO_3$ is doped with niobium pentaoxide ($Nb_2O_5$). A new phase further reported as $Nb_2Mo_3O_{11}$ or $3MoO_2{\cdot}Nb_2O_5$ (JCPDS 18-0840)[16] different from both oxides is observed upon increasing the $Nb_2O_5$ loading, and the layered structure of $MoO_3$ becomes nearly destroyed. This provided a stimulus to measure the dielectric properties and address the low frequency response manifested as a mild relaxation in the dielectric behaviour of such compounds. It is also of significance to explore the dielectric characteristics of this system, since it has not been studied before. More-

*For correspondence. (e-mail: scientific@aec.org.sy)

over, the electronic behaviour can strongly be influenced by the two-dimensional structural distortions which might affect the transport properties embedded in its response to external signals. This would as well be correlated to morphological transformations occurring upon doping, and this communication is an endeavour to study such characteristics.

The mixed ceramic oxides $Nb_2O_5$ + $MoO_3$ were elaborated as a powder via the solid state reaction method, for which the molar ratios $Nb_2O_5/MoO_3$ were taken to be 0.02, 0.03, 0.04, 0.05, 0.1, 0.2 and 0.4. Gradual heating of the mixture was then performed up to a temperature of 750°C (the melting point of $MoO_3$ is approximately 800°C) and the mixture was kept at this temperature for 4 h. The melt was cooled afterwards to room temperature, without observing any tangible reaction with the quartz tube. Powder X-ray diffraction (XRD) was performed on a STADI-P STOE Transmission Diffractometer, using CuK$\alpha$ radiation ($\lambda$ = 1.54059 Å), and a germanium monochromator operated at 50 kV and 30 mA. The XRD patterns were measured between 5° and 90° 2$\theta$, with a step size of 0.01 and a scanning speed of 0.5°/min. IR spectral measurements have also been performed to obtain information about the nature of the bonds in the studied samples. The powder was pressed as pellets for electrical measurements, and contact points were made on rectangular samples carved from these pellets using a conducting silver paint. T-type (copper–constantan) thermocouple was employed for accurate temperature sensing using the Keithley 2181A nanovoltmeter to read the voltage of the thermocouple. A primary check of the sample resistance was performed by means of a Keithley 614 electrometer, to ensure that good contacts exist in the sample. The AC conductivity experiments were carried out utilizing the HP 4192A LF impedance analyser, which tracks the impedance in the low frequency range between 5 Hz and 13 MHz. The latter produces a sinusoidal signal $V_{AC} = V_0 \cos \omega t$ from the internal oscillator with a maximum voltage $V_0$ = 1 V, and measures the voltage of the sample concomitantly via a four-point probe module. Hence the imaginary part of the dielectric function could accordingly be identified as a function of varying frequency and temperature.

The XRD patterns of the pure $MoO_3$ and mixed oxides $Nb_2O_5$ + $MoO_3$ with different molar ratios $Nb_2O_5/MoO_3$ are shown in Figure 1. It can be clearly observed that the samples doped with low molar ratio $Nb_2O_5/MoO_3$ up to 0.05 develop X-ray patterns (b–e) characteristic of non-doped $MoO_3$; notably with the most intense peaks, i.e. no new phases cropping up. The unit cell dimensions also tend to remain nearly unchanged for such low concentrations. This trend may be attributed to the fact that niobium fills initially the molybdenum vacancies present within the non-doped $MoO_3$. Thus no significant modifications in the structure of $MoO_3$ can be realized as long as the atomic radii of both elements (Mo and Nb) are close. On the other hand, Gaiger *et al.*[17], Hu and Davies[18] have demonstrated the existence of such vacancies in non-doped $MoO_3$. However, for molar ratio $Nb_2O_5/MoO_3$ in the range 0.05–0.2, the diffraction patterns f and g, in Figure 1 indicate new peaks besides the principal peaks of non-doped $MoO_3$. These additional peaks can be linked to the formation of a solid solution for which a novel phase disparate from the pure materials is forming. The peaks of this observed phase get more conspicuous with increasing the $Nb_2O_5$ loading (molar ratio = 0.4) as seen in Figure 1 h. As the molar ratio $Nb_2O_5/MoO_3$ increases beyond 0.4, the formation of the new phase is complete. We identify this phase as $Nb_2Mo_3O_{11}$ or $3MoO_2 \cdot Nb_2O_5$, since its diffraction peaks fit well the same phase of those peaks cited in the JCPDS[16], which also crystallize as a tetragonal system with unit cell parameters $\boldsymbol{a}$ = 23.100 and $\boldsymbol{c}$ = 9.0686. Since no diffraction peaks related to non-doped $Nb_2O_5$ are observed, it is possible that the dopant $Nb_2O_5$ wholly diffuses into $MoO_3$.

Figure 2 shows the FTIR spectra for the samples considered in Figure 1. The $MoO_3$ spectrum consists of a narrow band at 999 $cm^{-1}$, attributed to the valance vibrations of Mo=O band that is perpendicular to the layered structure of $MoO_3$. This spectrum also shows a broader band having a maximum at 820 $cm^{-1}$, which can be related to Mo–O valance vibrations of the Mo–O–Mo chains. There are two maxima in a wide absorption range as well; one at 630 $cm^{-1}$ and the other at 482 $cm^{-1}$ assigned to the lattice vibrations[19]. For samples with molar ratio $Nb_2O_5/MoO_3$ up to 0.1, it can be clearly observed that the bands pertaining to $MoO_3$ lattice keep appearing at the same frequencies. However, in the molar ratio $Nb_2O_5/MoO_3$ range of 0.1–0.2 the FTIR spectra develop new broad bands at 920, 780, 640 and 550 $cm^{-1}$ besides the $MoO_3$ bands. These bands can be ascribed to the vibration modes $v1$ and $v3$ of $(MoO_4)^{-2}$ shifted to the low wave-

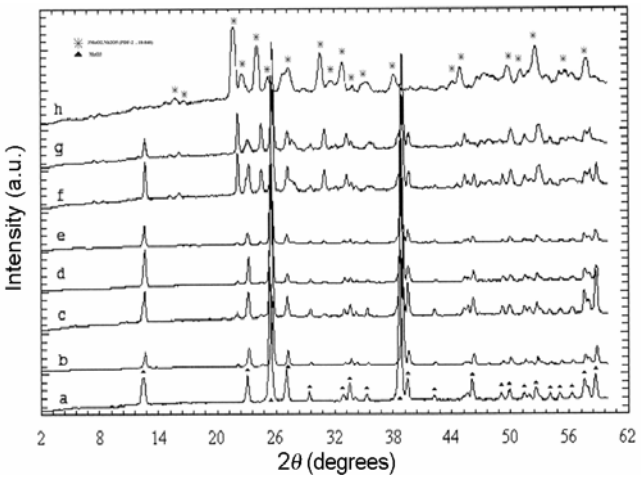


**Figure 1.** X-ray diffraction patterns of $Nb_2O_5$ + $MoO_3$ mixed ceramic oxides samples with molar ratios: (a) $Nb_2O_5/MoO_3$ = 0; (b) 0.02; (c) 0.03; (d) 0.04; (e) 0.05; (f) 0.1; (g) 0.2 and (h) 0.4.

number region due to bonding with Nb atoms. This may provide a supplement assertion to the formation of the new phase referred to in Figure 1. One can also see that in the molar ratio range of 0.5–0.2, the characteristic band of $MoO_3$ at 999 $cm^{-1}$ becomes broader, and completely disappears at the molar ratio value of 0.4. This is fundamentally due to the abolishment of the layered structure of $MoO_3$.

Over our range of temperatures, the imaginary part $\varepsilon''$ of the dielectric function of the ceramic system from the total AC conductivity $\sigma_{AC} = 2\pi f \varepsilon_0 \varepsilon''$ ($\varepsilon_0$ is the permittivity and $f$ the frequency) has been identified. Four molar ratios $Nb_2O_5/MoO_3$ have been picked out for AC electrical measurements: 0, 0.05, 0.2 and 0.4, corresponding to non-doped $MoO_3$, low $Nb_2O_5$ doping, during the start of formation of the new phase, and at the formation of the phase respectively. We initially studied the frequency response of the doped samples at a constant temperature in a span of the applied signal frequency with amplitude of 1 V, starting at a few hertz up to 13 MHz. Having recorded this response, three appropriate frequencies, 50 kHz, 500 kHz and 5 MHz, were selected to drive each sample and measure $\varepsilon''$ as a function of temperature ($80 \le T \le 300$ K). Figure 3 illustrates the response of non-doped $MoO_3$ taken as a logarithmic scale of the impedance versus frequency at room temperature. It can be clearly seen that the impedance tends to incline in a relaxed fashion starting linearly at low frequencies, and showing a reciprocal behaviour afterwards with increasing frequency. The same trend is found for the rest of the doped samples, and the inset in Figure 3 demonstrates the same for the molar ratio of 0.4. In order to measure the dielectric constant as function of temperature, we chose a frequency in the low range (50 kHz) where a variation in the sample response occurs, and then higher frequencies at 500 kHz and 5 MHz, as shown in Figure 4. It is obvious that at all frequencies and for all molar ratios $\varepsilon''$ is monotonously decreasing with reducing temperature and plummeting below 100 K (clearly seen at 50 kHz), and the insets reveal such a behviour for each curve separately. Also, $\varepsilon''$ has marginally higher values at 50 kHz than at the other two frequencies. The system shows a similar frequency response for the molar ratio of 0.05, as seen in Figure 5. For the molar ratio of 0.2, Figure 6 shows the dielectric constant curves at the selected frequencies. At 50 kHz the response remains as before, while at 500 kHz and 5 MHz, the $\varepsilon''$ curves are close to each other relaxing at around 95 K. Remarkably and unprecedently at the molar ratio of 0.4 (Figure 7), the dielectric response at 5 MHz acquires higher values than at 500 kHz, showing an anomalous small peak at around 230 K and then decreasing afterwards. This anomaly may be attributed, as we demonstrate later, to both an intrinsic mechanism and oxide doping[20]. Each curve at the selected frequency is also plotted individually in the insets of Figure 7.

For comparison, we plot the dielectric response curves for different molar ratios of doped samples at the selected frequencies. Figure 8 shows $\varepsilon''$ as a function of temperature for the four doping ratios at 50 kHz. One can unequivocally observe that the dielectric response at this frequency is the highest for the molar ratio 0.05, and tangible difference in $\varepsilon''$ values exists between the non-doped $MoO_3$ and the 0.05 samples. Further, the dielectric

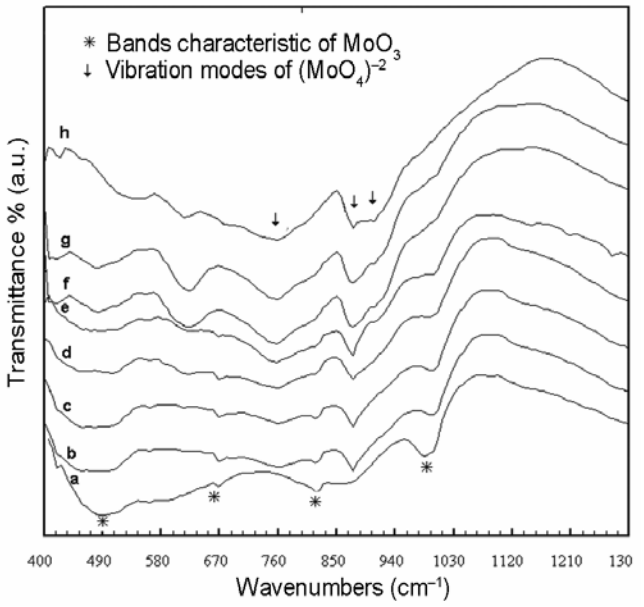


**Figure 2.** FTIR spectra of $Nb_2O_5$ + $MoO_3$ mixed oxide samples with molar ratios: (a) $Nb_2O_5/MoO_3$ = 0; (b) 0.02; (c) 0.03; (d) 0.04; (e) 0.05; (f) 0.1; (g) 0.2 and (h) 0.4.

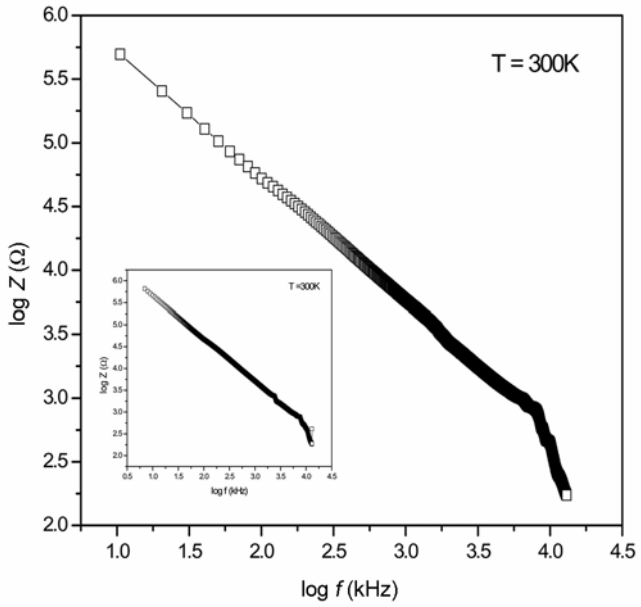


**Figure 3.** The non-doped $MoO_3$ electric impedance versus frequency on logarithmic scale at 300 K. (Inset) The same plot for doping molar ratio of 0.4.

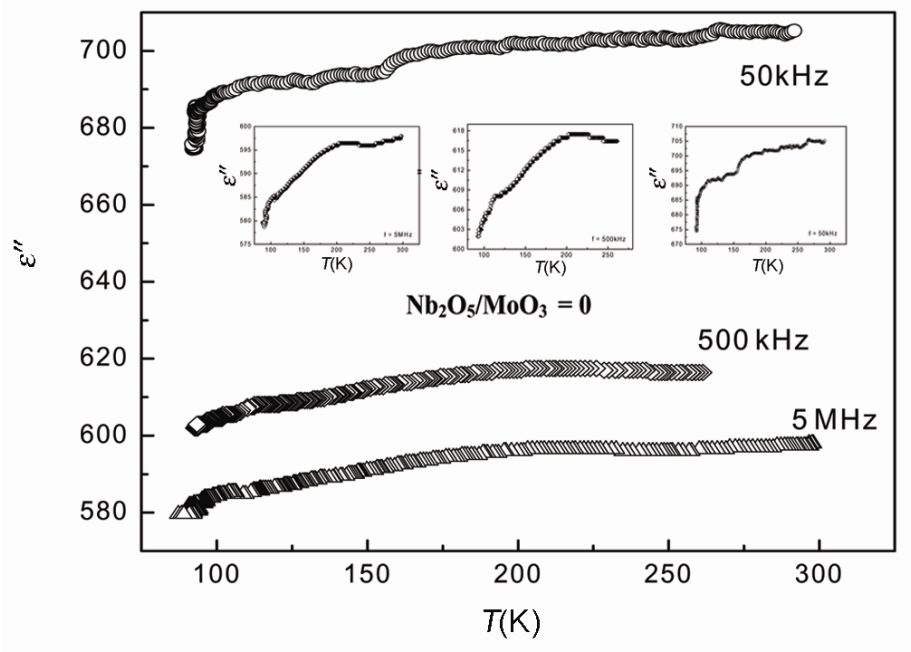


**Figure 4.** The complex dielectric susceptibility $\varepsilon''$ curves as a function of temperature for the non-doped $MoO_3$ sample at three frequencies: 50 kHz, 500 kHz and 5 MHz. (Inset) $\varepsilon''$ versus $T$ at each frequency separately.

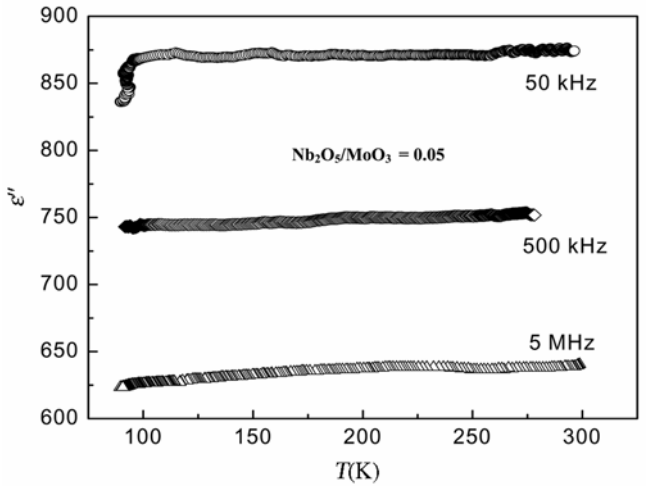


**Figure 5.** The complex dielectric susceptibility $\varepsilon''$ as a function of temperature for the 0.05 doped sample at three frequencies: 50 kHz, 500 kHz and 5 MHz.

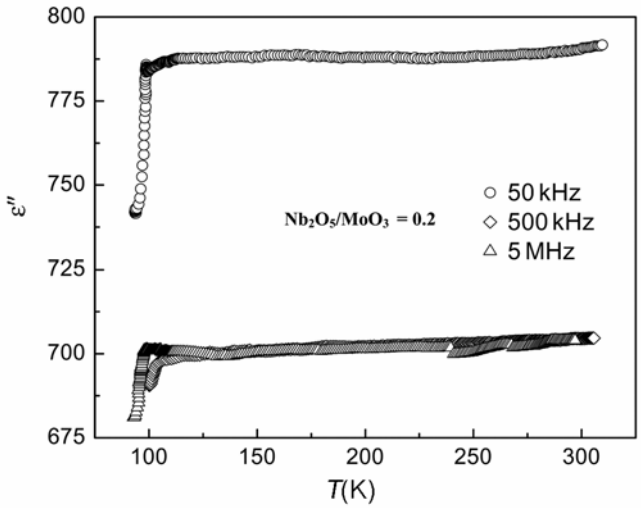


**Figure 6.** The complex dielectric susceptibility $\varepsilon''$ as a function of temperature for the 0.2 doped sample at three frequencies: 50 kHz, 500 kHz and 5 MHz. The curves come closer to each other for 500 kHz and 5 MHz and relax at around 95 K.

curves for the 0.2 and 0.4 molar ratios are close to each other, with $\varepsilon''$ having lower values for 0.4. The samples maintain the same behaviour at 500 kHz as shown in Figure 9. Yet the values of $\varepsilon''$ become smaller overall than at 50 kHz. The tendency of $\varepsilon''$ to drop can clearly be seen in Figure 10 for the 0 and 0.05 molar ratios at the higher frequency (5 MHz). The curve corresponding particularly to the 0.05 doped samples has significantly reduced, while those related to the 0.2 and 0.4 molar ratios have markedly scaled up, with an exceptionally pronounced dielectric maximum for the 0.4 molar ratio.

The strongly anisotropic $MoO_3$ ceramic is usually insulating at room temperature. The propensity towards forming bonds between the Mo atom and oxygen ensures filling completely the vacant bands of Mo with electrons. Moreover, with the availability of openings between the $MoO_6$ octahedron of the lattice, smaller atoms such as Nb could slide through it. This leads to improvement in the ionic conductivity. In the studied $Nb_2O_5 + MoO_3$ system, the dopant ($Nb_2O_5$) concentration increases gradually so that a significant contribution to the transfer of the 5s band electrons of Nb atoms to the unfilled 4d band of Mo

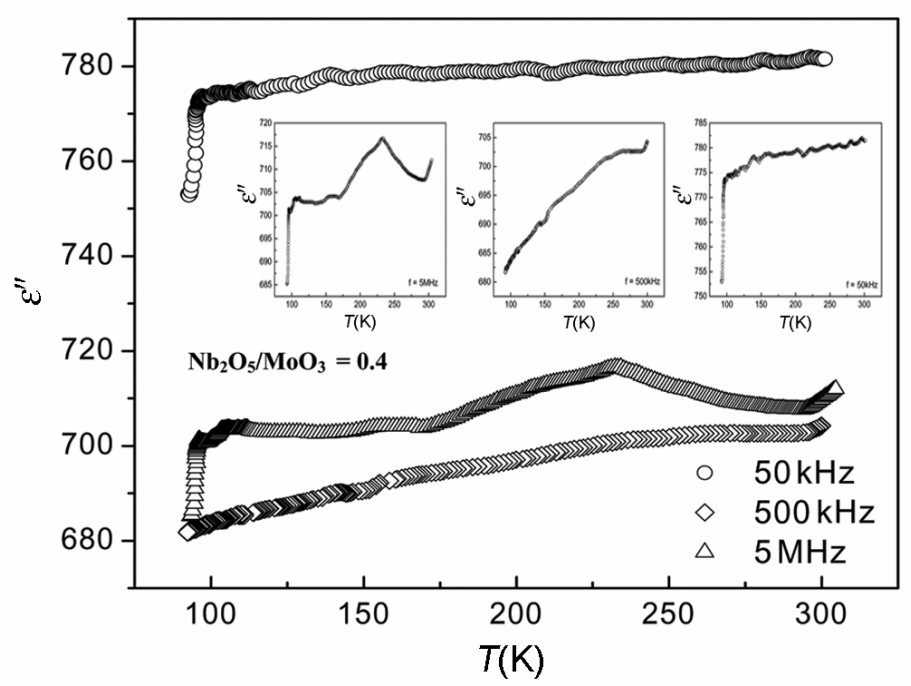


**Figure 7.** The complex dielectric susceptibility $\varepsilon''$ response as a function of temperature for the 0.4 doped sample at three frequencies: 50 kHz, 500 kHz and 5 MHz. The anomalous small dielectric 5 MHz peak can be seen at nearly 230 K. (Inset) Dielectric susceptibility at each frequency, and the maximum at 5 MHz is clearly observed after which $\varepsilon''$ rapidly decreases.

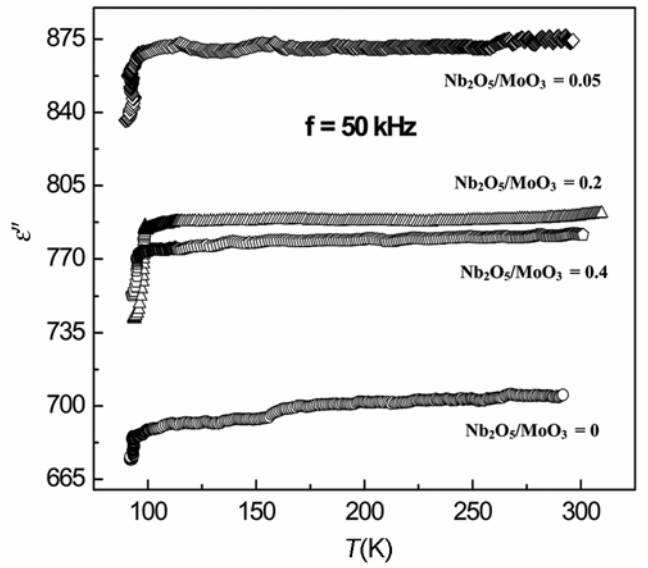


**Figure 8.** The complex dielectric susceptibility $\varepsilon''$ response as a function of temperature plotted for four doping concentrations: 0, 0.05, 0.2 and 0.4 at 50 kHz. $\varepsilon''$ is highest for 0.05, while the curves are close to each other for 0.2 and 0.4.

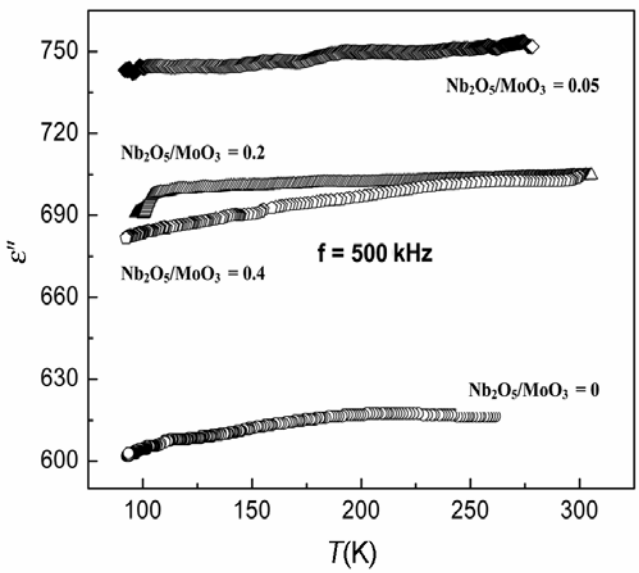


**Figure 9.** The complex dielectric susceptibility $\varepsilon''$ as a function of temperature plotted for four doping concentrations: 0, 0.05, 0.2 and 0.4 at 500 kHz.

atoms also occurs. Thus mounting participation of the $\pi$ p electrons of oxygen atoms in the electrostatic attraction corresponding to the Mo 4d–O2p ligand also takes place. The resultant improvement in conductivity particularly at low temperatures, is associated with a structural phase transition owing to exceeding the $Nb_2O_5$ loading and reducing $MoO_3$ in addition to excess oxygen vacancies available in the system. The general trend of the samples is justified with such interpretation as they exhibit a gradual decrease in the dielectric response, clearly seen for each concentration (Figures 4–7). At low temperature ($T < 100$ K), a slight relaxation is manifested particularly

at the low frequency (50 kHz), and is more pronounced for the 20% and 40% doping (Figures 6 and 7); this can be attributed to ionized oxygen vacancies[20]. This behaviour is also in qualitative agreement with space-charge model accounting for dielectric relaxation reported previously in perovskites such as $PbMg_{1/3}Nb_{2/3}O_3$ or $Pb(Zr,Ti)O_3$ in the low-frequency and high-temperature range[21,22]. As common to many dielectric materials, the free carriers stored at the dielectric electrode interfaces can lead to space charge[23]. Hence, macroscopic dipoles are formed upon the application of an electric field, which breaks the symmetry of this space charge. In addition, a dielectric maximum was found in numerous samples (most prominent at 1 kHz between 500 and 600 K). This anomaly has been shown to stem from a Debye dielectric dispersion which mildly diminishes following a thermally activated Arrehenius law:

$$\tau = \tau_0 \exp(E_\tau / k_B T), \quad (1)$$

where $\tau = 1/2\pi f$ and $\tau_0$ are the Debye and high temperature relaxation times respectively, and $E_\tau$ the activation energy. Moreover, the observed dielectric peak between 200 and 300 K (Figure 7) and the unprecedented sample response for the molar ratio of 0.4 at 5 MHz are in favour of the diffuse dielectric anomaly[21]. The latter is ascribed to the easing and broadening of a dielectric response in the frequency domain for which a relaxation due to polarized intrinsic nanoregions in the lattice both below and above the diffuse transition temperature occurs. As the electric dipoles are strongly influenced by lattice defects[24], depending on the compositional and structural fluctuations within the sample, this anomaly can be manifested. In view of the data presented in this communication, one can propose that on increasing the doping content, more ionized oxygen vacancies corresponding to $(MoO_4)^{-2}$ develop thus leading to relaxing dipoles. These dipoles are related to the density of oxygen vacancies, and consequently the observed decrease in dielectric response with reducing temperature has to follow the conductivity, where the complex conductivity $\sigma''$ is a function of $\omega$. On the other hand, the motion of oxygen vacancies may not be restricted to one unit cell, but can be non-localized and spread out to the entire sample resulting in ionic conductivity and ill-defined relaxing dipoles[21].

In this communication, ceramic samples of $MoO_3$ doped with different concentrations of $Nb_2O_5$ oxide have been prepared. The X-ray and FTIR data revealed a structural transformation in the system upon doping up to 0.4 molar ratio, resulting in a new discernible phase proposed as an isotype of $Nb_2Mo_3O_{11}$ or $3MoO_2{\cdot}Nb_2O_5$. We have measured the dielectric properties of these samples corresponding to four dopant concentrations, 0, 0.05, 0.2 and 0.4, at three frequencies, i.e. 50 kHz, 500 kHz and 5 MHz of the drive signal. Transport measurements on the samples have shown that for doping concentration 0, 0.05 and 0.2, the complex dielectric function monotonously decreased with reducing temperature, yielding the lowest response at the highest frequency (5 mHz). In contrast, for the 0.4 doped samples the system extraordinarily exhibited anomalous dielectric response at 5 MHz, so that it acquired higher values than before, yet with a maximum appearing in the range 200–300 K. The latter maximum has been qualitatively interpreted on the grounds of excess oxygen vacancies that give rise to relaxing dipoles with increased doping, associated with improvement in ionic conductivity that follows a thermally activated mechanism. Further studies are necessary to uncover the physical nature of a such system, particularly its ferroelectric relaxation at higher frequencies, which can be useful in practical applications.

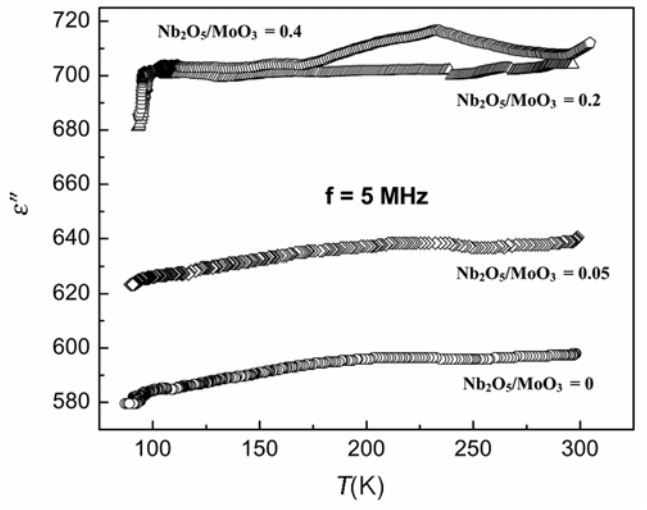


**Figure 10.** The complex dielectric susceptibility $\varepsilon''$ response as a function of temperature plotted for four doping concentrations: 0, 0.05, 0.2 and 0.4 at 5 MHz. The tendency of $\varepsilon''$ values to drop is clearly observed at this frequency, and the curves corresponding to the 0.2 and 0.4 doping are scaled up with pronounced dielectric maximum at 0.4.


1. Haber, J. and Lailk, E., Catalytic properties of $MoO_3$ revisited. *Catal. Today*, 1997, **33**, 119–137.
2. Kitao, M., Yamada, S., Hiruta, Y., Suzuki, N. and Urbe, K., Electrochromic absorption spectra modulated by the composition of $WO_3/MoO_3$ mixed films. *Appl. Surf.*, 1988, **33–34**, 812–817.
3. Reddy, B. M., Chary, K. V. R., Subrahamayan, V. S. and Nag, N. K., Characterization of sulphided molybdenum-containing hydroprocessing catalysts by oxygen and hydrogen chemisorptions. *J. Chem. Soc. Faraday Trans.*, 1985, **81**, 1655–1667.
4. Ng, K. Y. S. and Culari, E., Molybdena on titania: II. Thiophene hydrodesulfurization activity and selectivity. *J. Catal.*, 1985, **95**, 33–40.
5. Masuoka, Y., Niwa, N. M. and Murakami, Y., Morphology of molybdena supported on various oxides and its activity for methanol oxidation. *J. Phys. Chem.*, 1990, **94**, 1477–1482.
6. Zhang, W., Desikan, A. and Oyama, S. T., Effect of support in ethanol oxidation on molybdenum oxide. *J. Phys. Chem.*, 1995, **99**, 14468–14476.

7. Williams, C. C., Ekerdj, J. G., Jehng, J. M., Hardcastle, F. D. and Wachs, I. E., A Raman and ultraviolet diffuse reflectance spectroscopic investigation of silica-supported molybdenum oxide. *J. Phys. Chem*., 1991, **95**, 8781–8791.
8. Chen, K., Xie, S., Igesia, E. and Bell, A. T., Transition metal oxide chemistry: electronic structure study of $WO_3$, $ReO_3$, and $NaWO_3$. *J. Catal*., 2000, **198**(2), 232–242.
9. Corà, F., Stachiotti, G. and Catlow, A., Structure and properties of oxidative dehydrogenation catalysts based on $MoO_3/Al_2O_3$. *J. Phys. Chem. B*, 1997, **101**, 3945–3952.
10. Schneemeyer, L. F., DiSalvo, F. J., Spengler, S. E. and Waszczak, J. V., Dramatic impurity effects on the charge-density wave in potassium molybdenum bronze. *Phys. Rev. B*, 1984, **30**(8), 4297–4301.
11. Jie, Y. and Ong, N. P., Low-temperature, low-frequency dielectric response of the pinned charge-density wave in $K_{0.3}MoO_3$. *Phys. Rev. B*, 1991, **44**(15), 7912–7916.
12. Littlewood, P. B., Screened dielectric response of sliding charge-density waves. *Phys. Rev. B*, 1987, **36**, 3108–3116.
13. Machado-Charry, E. *et al.*, Analysis of the scanning tunnelling microscopy images of the charge density wave phase in quasi-one-dimensional $Rb_{0.3}MoO_3$. *Phys. Rev. B*, 2006, **74**, 155123–155128; arXiv:cond-mat/0606694.
14. Stokes, J. P., Robbins Mark, O. and Bhattacharya, S., Ac response of pinned-charge-density-wave conductors. *Phys. Rev. B*, 1985, **32**(10), 6939–6941.
15. Chen, A., Scott, J. F., Zhi, Y., Ledbetter, H. and Baptista, J. L., Dielectric and ultrasonic anomalies at 16, 37, and 65 K in $SrTiO_3$. *Phys. Rev. B-II*, 1999, **59**(10), 6661–6664.
16. Joint Committee on Powder Diffraction Standards 2004, JCPDS-PDF, Card No. 18-0840.
17. Caiger, N. A., Crouch-Baker, S., Dickens, P. G. and James, G. S., Preparation and structure of hexagonal molybdenum trioxide. *J. Solid State Chem*., 1987, **67**, 369–373.
18. Hu, Y. and Davies, P. K., Acid-leaching of sodium brannerite: synthesis and structure of $Na_{0.13}(V_{0.13}Mo_{0.87})O_3 \cdot nH_2O$. *J. Solid State Chem*., 1995, **119**, 176–190.
19. Dieterle, M., Weinberg, G. and Mestl, G., Raman spectroscopy of molybdenum oxides. Part I. Structural characterization of oxygen defects in $MoO_{3-x}$ by DR UV/VIS, Raman spectroscopy and X-ray diffraction. *Phys. Chem. Chem. Phys*., 2002, **4**, 812–821.
20. Chen, A., Zhi, Y., Lunkenheimer, P., Hemberger, J. and Loidl, A., Dielectric relaxation modes in bismuth-doped $SrTiO_3$: The relaxor behavior. *Phys. Rev. B-II*, 1999, **59**(10), 6670–6674.
21. Bidault, O., Goux, P., Kchikech, M., Belkaoumi, M. and Mgilone, M., Space-charge relaxation in perovskites. *Phys. Rev. B-II*, 1994, **49**(12), 7868–7873.
22. Bidault, O., Maglione, M., Actis, M. and Kachikech, M., Polaronic relaxation in perovskites. *Phys. Rev. B-II*, 1995, **52**(6), 4191–4197.
23. Jonscher, A. K., *Dielectric Relaxation in Solids*, Chelsea, New York, 1983.
24. Ormancey, G., Thèse d'Etat, Dijon, 1978.

ACKNOWLEDGEMENTS. We thank Prof. I. Othman, The Director General of the Atomic Energy Commission of Syria, Syria for support. We also thank Dr T. Yassin, Head, Department of Chemistry and Dr R. Darwich for their valuable suggestions, and F. Nasrallah and S. Kanaan for technical assistance.

Received 11 June 2009; revised accepted 5 September 2011

# Lithospheric structure across the western part of the Narmada–Son Lineament from wide-angle seismic data

**A. R. Sridhar, A. S. S. S. R. S. Prasad, Kalachand Sain* and Dipankar Sarkar**

CSIR-National Geophysical Research Institute, Uppal Road, Hyderabad 500 007, India

**Seismic refraction and wide-angle reflection data were acquired in early 1980s in analog form along a 260-km long Sendhwa–Sindad DSS profile over the Deccan Traps-covered area across the Narmada–Son Lineament. The data with 15 Hz high cut filter were later digitized and assembled into record sections which exhibit deep-travelling, identifiable, wide-angle reflected phases by playing with gain. We have derived the lithospheric velocity structure in Central India by kinematic and dynamic modelling of these phases. The result shows two intra-crustal discontinuities, one at a depth of 14.5–16.5 km and the other at 26 km, where velocity jumps from 6.6 to 7.0 km/s. The sub-crustal lithosphere beneath a crust–mantle boundary at 39–41 km consists of two prominent low-velocity (7.0 km/s) zones bounded by high-velocity (8.0–8.2 km/s) layers.**

**Keywords:** Crust–mantle boundary, lithosphere, ray tracing, seismic refraction, wide-angle reflection.

THE lithospheric velocity structures can be determined by the earthquake or the explosion seismology data. The crustal and upper mantle structures have been derived in various geological settings of the world using long-range seismic refraction/wide-angle seismic data by several workers[1,2]. We derive the lithospheric velocity structure by kinematic and dynamic modelling of such wide-angle seismic data iteratively using a ray-tracing software[3]. The velocity structure in different regions of the Indian peninsula is known from travel-time modelling of earthquakes[4], surface wave dispersion[5–7], waves spectra[8] and deep seismic sounding (DSS)[9–12] studies.

As a continuation of crustal seismic studies[13], four DSS profiles, each of about 250 km long, were shot across the Narmada–Son Lineament (NSL) in Central India. This lineament is the most conspicuous linear geological feature in India after the Himalaya. It passes through Broach on the west coast of India in NNE–SSW direction cutting across the whole of Central India and has been periodically reactivated since the Precambrian[14,15]. The crustal velocity models derived from the DSS data acquired along these profiles across the NSL reveal, in general, a high positive velocity gradient up to a depth of about 10 km from the surface. The Moho is found to vary

*For correspondence. (e-mail: kalachandsain@yahoo.com)